Radio Science

RESEARCH ARTICLE
10.1029/2023RS007758

Suppresion of Log-Periodic Dipole Antenna Spurious Radiation by Lumped Element Loading for Radioastronomical Application

Georgios Kyriakou[1,2], Pietro Bolli[1], and Lorenzo Mezzadrelli[3]

[1]Arcetri Astrophysical Observatory, National Institute for Astrophysics, Florence, Italy, [2]Department of Physics and Astronomy, University of Florence, Florence, Italy, [3]Sirio Antenne, Volta Mantovana, Italy

Key Points:

- A spurious radiation problem of the log-periodic dipole antenna used for Square Kilometer Array-Low affects its performance with respect to spectral smoothness
- A solution is proposed by means of loading the affected dipoles with appropriately designed parallel RLC circuits
- Experimental verification using measured scattering parameters in the near-field of a two-antenna system is provided

Correspondence to:
G. Kyriakou,
georgios.kyriakou@inaf.it

Citation:
Kyriakou, G., Bolli, P., & Mezzadrelli, L. (2023). Suppresion of log-periodic dipole antenna spurious radiation by lumped element loading for radioastronomical application. *Radio Science*, *58*, e2023RS007758. https://doi.org/10.1029/2023RS007758

Received 22 MAY 2023
Accepted 8 AUG 2023

Author Contributions:
Conceptualization: Georgios Kyriakou, Pietro Bolli
Data curation: Georgios Kyriakou
Formal analysis: Georgios Kyriakou
Funding acquisition: Pietro Bolli
Investigation: Georgios Kyriakou, Pietro Bolli, Lorenzo Mezzadrelli
Methodology: Georgios Kyriakou, Pietro Bolli
Project Administration: Pietro Bolli, Lorenzo Mezzadrelli
Resources: Pietro Bolli, Lorenzo Mezzadrelli
Software: Georgios Kyriakou, Pietro Bolli
Supervision: Pietro Bolli
Validation: Georgios Kyriakou, Pietro Bolli
Visualization: Georgios Kyriakou

Abstract Log-Periodic Dipole Antennas have been known to provide good performance over large fractional bandwidths. However, optimized designs of log-periodic antennas, in particular for radioastronomy and remote sensing, need to tackle the spurious radiation of secondary dipole harmonics that can compromise the gain smoothness and therefore the ability to detect natural spectral features emitted by the probed sources. A new, low-cost method applicable also at a post-design stage is proposed in this paper, which relies on loading some of the dipoles with appropriate lumped circuit elements in order to avoid this unwanted feature while preserving the desired performance characteristics. Application is found on the log-periodic dipole antenna selected for the low-frequency instrument of the SKA (Square Kilometer Array), and general guidelines are described for other designs. An experimental test using a transmitting VHF antenna and the antenna under test with new RLC loaded dipoles confirms our solution.

1. Introduction

Log-Periodic Dipole Antennas (LPDA) (Carrel, 1961) are a standard and useful type of antennas, and they have been used in many applications and frequency bands due to their advantage of simple geometry (dipoles) and variety of construction methods (solid tubes, 2D microstrip printings), as well as their ability to form arrays and enhance the sensitivity of the resulting instrument (Isbell, 1960). Ever since their introduction, they have been the subject both of theoretical treatment (Bantin & Balmain, 1970; Cheong & King, 1967), as well as application-driven design, notably in Mistry et al. (2021) with low-frequency extension modifications (as in the hereto examined antenna). In the early years of log-periodic antenna design, where computational resources were limited, theoretical work was the basis of understanding the log-periodic parameters, and a number of standard tools guided their choice (among which the optimum $\sigma - \tau$ curve, the bandwidth vs. opening angle α (Carrel, 1961) etc.). Of special interest for the resonant behavior of LPDAs, as examined in this work, are also the early theoretical derivations of the log-periodic cell, that constitute a near-field model of the antenna for evaluation of its reflection, a parameter expected to be log-periodically repeatable (DuHamel & Armstrong, 1966; Jones & Mayes, 1969). More recent work (McLean et al., 2014) has used these results to describe the stop-region of an LPDA, comparing it to modern accurate simulations.

In this paper, we will examine the problem of spurious radiation in LPDAs (Hilbert et al., 1989) as well as a new technique of loading the antenna dipoles to dissipate the second order mode power on a resistor appropriately chosen as part of an RLC parallel circuit. The SKALA4.1 antenna (Bolli, Mezzadrelli, et al., 2020) will work as an example to assess the performance both in terms of simulation and experimental measurement, but the concept is generalized for all similar antennas, that is, LPDA with non straight-wire dipoles.

SKALA4.1 is a dual polarized active log-periodic antenna, with a bottom-placed bow-tie dipole, and will be operational in the frequency range of 50–350 MHz (Bolli, Mezzadrelli, et al., 2020). It is the evolution of previous designs, such as SKALA-2 (de Lera Acedo et al., 2015), SKALA3 (de Lera Acedo & Wackley, 2017) and has been selected by the SKAO (https://cdr.skatelescope.org/\#milestones?lfaa) for construction. An electromagnetically simplified model used for this study has also been described in Steiner et al. (2020). The radio telescope SKA-Low will be comprised by 512 stations of 256 SKALA4.1 antennas each and is going to be the most sensitive radio telescope ever built in this frequency range (Labate, Dewdney, et al., 2017). Despite the antenna having surpassed all major evaluation criteria, the problem of narrow gain discontinuities (or so-called glitches) has persisted, and this was the starting point of our present analysis.

Writing – original draft: Georgios Kyriakou
Writing – review & editing: Georgios Kyriakou, Pietro Bolli, Lorenzo Mezzadrelli

The problem of narrow-band glitches, although minor for other applications, could potentially sever the narrow-band astronomical observations conducted with the SKA-Low (Labate, Braun, et al., 2017). Confident signal detection in radioastronomy requires a high degree of spectral purity, since the sought-out signals are weak. In the case of spectral lines (highly redshifted molecular or recombination lines, for meter wavelengths where SKA-Low will operate), acute features such as those we examine mimic them in the data. Furthermore, polynomial fitting and extraction techniques that work well in slowly varying instrumental anomalies cannot be applied in such narrow frequency bands, since they would also dampen the useful signal. The need for antenna hardware solutions, therefore, emerges for such problematic features.

While it is certainly desired, after the latest SKA Critical Design Review, to propose minimal changes to this antenna, a technique that does not set decisive constraints in an initial design process, rather corrects such spurious behavior of LPDAs at a post-design phase, is not present in the current literature. Our method in this paper mainly answers to the challenging scientific requirements of a complex project such as the SKA-Low. Due to its low-cost and post-design implementation, though, it is also an attractive method for other applications such as remote sensing.

The paper is organized as follows: Section 2 describes the problem of spurious radiation in LPDA and introduces the parallel RLC load solution, Section 3 examines its effect on the antenna performance in each log-periodic operating frequency region, and Section 4 presents the simulation results of the implementation on a SKALA4.1 antenna and its constituent dipoles. In Section 5 we present an experimental test conducted using a SKALA4.1 and a VHF antenna, using both loaded and unloaded dipoles to verify the method; the method followed relies on the simulated performance but no direct comparison can be made with the previous simulated gain results. Section 6 outlines our conclusions.

2. Spurious Radiation Phenomenon and Lumped Element Loading

The problem of spurious radiation in this type of antennas has been described by some authors, citing mostly asymmetry concerns (Balmain & Nkeng, 1976) as well as the finiteness of the structure and the associated termination (Gong & Balmain, 1986; Hilbert et al., 1989). In most types of applications, though, such problems did not cause significant degradation of the performance, as their impact was mostly tackled by choosing a high input impedance (De Vito & Stracca, 1973).

In this paper, we are looking into a different spurious radiation phenomenon, which has been hinted at by Hilbert et al. (1989), and does typically appear in non-straight dipole elements; it originates from second order modes of these dipoles, which are undesired for the performance of the antenna. The active region of an LPDA where dipoles are excited with their primary mode (dipole length $l \approx \lambda/2$) is not perfectly matched to the feeding line impedance, while there are also dipoles in the operating frequency range for which the condition of length approaching λ occurs. Power leaks in the non-active regions being reflected back from the primary-mode excited active dipoles, and excites this secondary mode ($l \approx \lambda$) after propagating further down the boom to the longer dipoles, creating a second active region. For a SKALA4.1 antenna, this problem has been described and experimentally measured in Kyriakou et al. (2021). In general, non straight-wire dipoles do not have the boundary condition of zero current at their edge, and their second order mode can have non-zero value at their middle. This mode can therefore be excited with a middle-placed port, which would not be possible for straight-wire dipoles (see also Figure 2b).

It should be noted that, many other techniques already proposed in literature, such as the choice of different length to radius ratios l_n/a_n, a variable boom characteristic impedance Z_0 or dipole separation d_n (Gong & Balmain, 1986; Hassan et al., 1991) have been proven insufficient or limited by more prioritized specifications in our examined antenna. For example, even though the input impedance of the SKALA4.1 is prioritized to be matched to 50 Ω as best as possible, a boom of varying Z_0 does not violate this requirement if a non-constant z-profile of the boom cross-section is chosen. Such attempts were made with constant, linear, parabolic boom profiles and combinations thereof, but were eventually not proven fruitful in tackling spurious radiation. A different shape of the dipoles besides the triangular, as in Balmain & Nkeng (1976), was also an attempted solution, but apart from significantly changing the antenna geometry, it was again proven an unsuccessful redesign option. Indeed, as has been shown in Jones & Mayes (1969) this is a complex problem involving both Z_0 and the dipole impedances.

Attempts at lumped element loading by using inductive or capacitive loads have already been made in a number of works, even for slot-antenna radar applications, as in Zhao et al. (2018). Most relevant to ours Sheng and

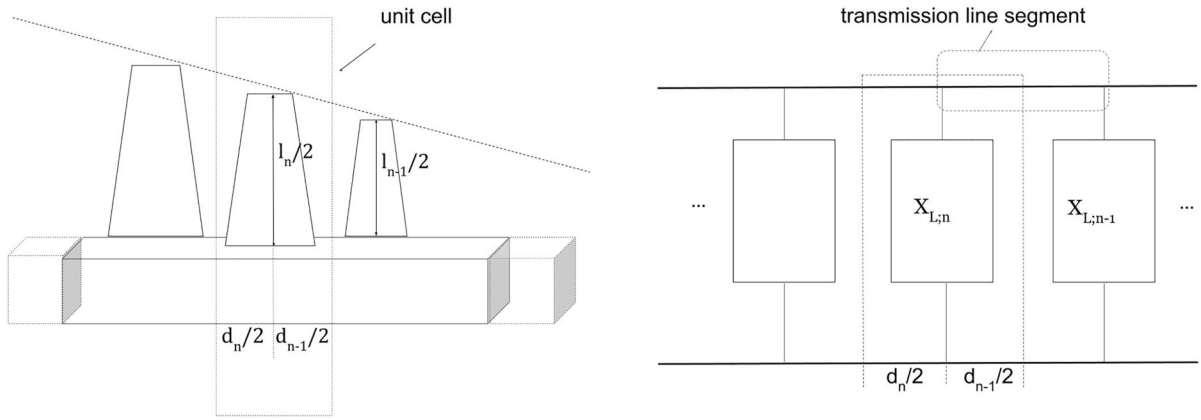

Figure 1. (a) Log-periodic cell of an Log-Periodic Dipole Antennas (LPDA) configuration, including the dipole of arbitrary shape and the boom segment to which it is connected (dimensions are also shown), (b) The equivalent circuit model of (a) in non-resonant regions of the LPDA.

Chen (2019) and Liang and Wu (2018), used an inductance to suppress such undesired modes but in a 2-dipole configuration, while He et al. (2019) using a capacitive load aimed mostly at improving the reflection coefficient of the designed antenna. The choice of an RLC load as a bandstop circuit in this work is made both for simplicity of design as well as for practical reasons relating to phase stability. An RLC circuit is a well-understood element and has also found application in other types of antennas, such as to reduce mutual coupling in arrays. The position of such a circuit in any antenna design has to be integrated in such a way so as not to interfere with antenna performance. For resonant antennas, this mainly means the primary modes; as will be proven in the following section, in our case the placement should correspond to the maximum of the secondary dipole mode current distribution. Thus, the novelty of this paper is the integration of this lumped circuit in the dipoles of an LPDA: a careful analysis is conducted in the realization of the circuit to overall maintain the mechanical and electrical characteristics of the antenna.

Our goal in the following section is to generalize this method in all LPDAs using non-straight wire dipoles, with respect to achieving gain smoothness, while keeping the reflection coefficient identical for all practical purposes. The cost on radiation efficiency should also be minimum.

3. Effect of Parallel RLC Load in LPDA Regions

In this section, we consider all dipoles of an LPDA as potentially loaded with an RLC circuit, while application is found usually only on some of them, depending on the operating frequency range of the antenna. We shall examine the effect of dipole loading with an RLC parallel circuit in the frequency regions where the dipoles of an LPDA are non-resonant and the regions where the dipoles resonate with their primary or secondary mode. In all of these regions some approximations can be made both on the behavior of the RLC load and the main function of the log-periodic "cells." One such cell is a dipole and a segment of the boom as transmission line, and is the unit element which is scaled in the log-periodic configuration, as can be seen in Figure 1a where 3 cells are shown to highlight the cross-feeding of consecutive dipoles (by the symmetric boom conductor - not shown). All these cells connected as a network appear, approximately, either as continuously scaled transmission line segments (propagating power) or equivalent resonant circuits themselves (radiated power), or a combination of both (Jones & Mayes, 1969).

3.1. Non-Resonant Regions

We first introduce a dipole indexing using an increasing n, from shorter to longer elements on an LPDA. If the wavenumber is $k = \omega/c_0$, then in the region $kl_n < \pi$, we expect all dipoles 1 through n to be short and thus to not radiate (the exact bound depends on the dipole's parameters). For an LPDA, this region "moves" when focusing on a different frequency. As has been shown in Carrel (1961) and DuHamel and Armstrong (1966), these dipoles load in parallel the boom transmission line, in this case capacitively. If a log-periodic cell n has an equivalent

Table 1
First and Second Dipole Resonance Frequencies and Electric Lengths for a SKALA4.1 Antenna

Dipole n	15	16	17	18	19
$f_{n,1}$ (MHz)	149	133	118	107	95
$f_{n,2}$ (MHz)	318	284	255	229	206
$l_n/\lambda_{n,1}$	0.477	0.473	0.464	0.462	0.456
$l_n/\lambda_{n,2}$	1.02	1.01	1.00	0.99	0.99

transmission line inductance $L_{0,n}$, capacitance $C_{0,n}$ and thus characteristic impedance $Z_{0,n} = \sqrt{L_{0,n}/C_{0,n}}$, then the reactance added to the boom is:

$$X_{L,n} = -Z_{0,n}\cot\left(\frac{kl_n}{2}\right) \tag{1}$$

A circuit equivalent of the log-periodic dipole antenna in its non-resonant region can be seen in Figure 1b. Following the same indexing as that of the dipole it is potentially attached to, the parallel nth RLC load has a complex value:

$$Z_{RLC,n} = \frac{j\omega L_n R_n}{R_n(1-\omega^2 L_n C_n) + j\omega L_n} \tag{2}$$

and it is tuned at the second resonant frequency of its dipole such that:

$$\omega_{n,2} = \frac{1}{\sqrt{L_n C_n}} \tag{3}$$

In the low frequencies that we are examining, we will approximate it as an inductive load $j\omega L_n$, since $\omega^2 L_n C_n \ll 1$ and $R_n \gg \omega L_n$. This nth load, when attached to the dipole n, modifies $Z_{0,n}$ in a non-uniform way, perturbing the transmission line model. The inductance L_n has to be small with respect to $L_{0,n}$ and $1/\left(\omega_{n,2}^2 C_{0,n}\right)$ (approximate expressions of which can be inferred from McLean et al. (2014)), in order not to significantly affect the equivalent dipole characteristic impedance, and thus the added reactance to the boom.

In the frequency range, which according to the dipole n is approximately such that $\pi < kl_n < 2\pi$, we cannot employ the same transmission line model as in the short dipole region, because of the fact that we have non-negligible radiation which works as an end-effect on this transmission line. It should be clarified though that this region still propagates the power which has not been radiated due to non-perfect matching to the boom, even though the effect is more complicated. Lumped element non-dissipative loading of isolated dipoles in this region (as is also our case, since $Z_{RLC,n}$ can still be approximated as inductive), for straight wires, has been theoretically examined in Nyquist and Chen (1966). The dipole input impedance is dependent on the current through the lumped element, which is zero for a straight wire dipole—hence no effect would be visible—but close to zero for other elongated shapes, thus we are not expecting any significant differences with respect to how an unloaded dipole would behave in the log-periodic configuration.

3.2. Resonant Regions

In these frequencies, which are roughly around $kl_n \approx \pi$ or $kl_n \approx 2\pi$ respectively (see Table 1, rows $f_{n,1}, f_{n,2}$), the dipole radiates power in its primary or secondary mode. The approximation depends on the width of the dipole (thick or thin), as well as on the resonance region; in fact, in an LPDA closely spaced dipoles interact, causing the distinct resonance of each one to be away from its self-resonance. The most useful tool to assess their excitation is the quality factor. According to Yaghjian and Best (2005), the Q-factor of a resonant antenna at any resonant frequency ω_r of order r, is approximated as:

$$Q(\omega_r) = \frac{\omega_r |Z'(\omega_r)|}{2\Re\{Z(\omega_r)\}} \tag{4}$$

where $Z(\omega_r)$ denotes the complex impedance of the antenna, and the primed quantity is its derivative, at resonant frequency ω_r. It must be noted that this definition holds both for lossless and lossy antennas, by adding the losses as an equivalent term of the real part. For our loaded dipole case, as has been already mentioned, the best position to place the load is where the current excited at $\omega_{n,2}$ is maximum. This does not only stem from the intuitive fact that we want to suppress this current as efficiently as possible, but is also necessary if we want to not intercept power from the primary mode at $\omega_{n,1}$, whose current should be minimum at the same point. If the dipole has an elongated shape, a lumped impedance placed at both $x_n = \pm l_n/2$, that is, the ends along the largest dimension, satisfies this requirement.

Focusing on the second resonance of interest, $\omega_{n,2}$, our load is at its resonant frequency so we have exactly $Z_{RLC,n} = R_n$. We can therefore represent this equivalent loss resistance, according to Yaghjian and Best (2005), as:

$$R_{L,n}(\omega_{n,2}) = \left|\frac{I_n(\omega_{n,2}, l_n/2)}{I_n(\omega_{n,2}, 0)}\right|^2 R_n \tag{5}$$

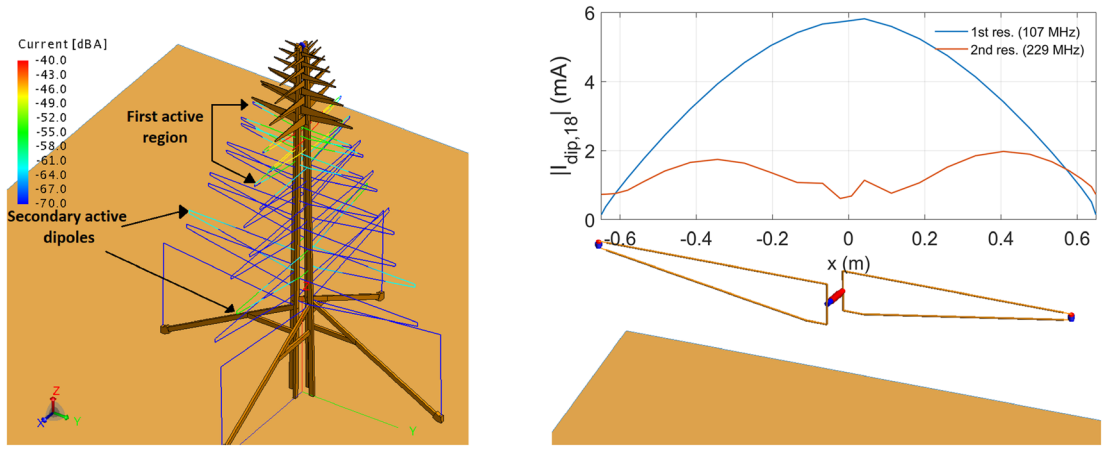

Figure 2. (a): A SKALA4.1 antenna excited at 229 MHz, geometry colored for wire current in dBA. Two active regions are discerned, with dipole 18 (counting from top to bottom) being the parasitic, (b): A FEKO schematic of triangular dipole 18 of SKALA4.1 over an infinite Perfect Electric Conductor surface, where 3 ports can be seen: a middle one for the voltage gap excitation as well as 2 edge ports where the loads are placed. Plotted are also the current distributions of the first and second resonances, as a function of the x coordinate, at 107 and 229 MHz respectively.

where $I_n(\omega_{n,2}, l_n/2)$ is the dipole current at the load placement and $I_n(\omega_{n,2}, 0)$ at the excitation point, at $\omega_{n,2}$. If we denote the nth dipole impedance as $Z_{dip,n}$ then for the loaded (and hence lossy at $\omega_{n,2}$) nth dipole the impedance of Equation 4 is indexed as $Z_n = Z_{dip,n} + R_{L,n}$. By the desired level of the Q-factor, our R_n is chosen. Note that in this factor there is an implicit assumption of tuning the antenna to its resonance such that $\Im\{Z(\omega_r)\} = 0$; away from self-resonance (or in an untuned antenna as in Yaghjian and Best (2005)) there exists some extremum of $\Re\{Z(\omega_r)\}$ such that $\Im\{Z'(\omega_r)\} > 0$. To find other meaningful representations of modal Q-factors of the antenna by tuning a specific modal reactance to zero one would need to resort to an internal energy formulation, as in the work of Capek (Capek et al., 2012).

4. Application on the SKALA4.1 Antenna

SKALA4.1 is a log-periodic antenna which features 19 triangular dipoles, a bow-tie dipole at its bottom, and a dual-conductor transmission line of rectangular cross-section as boom, while it is placed over a ground mesh which can be approximated as an infinite Perfect Electric Conductor (PEC). It is a dual-polarized antenna, but with a very low level of cross-coupling, so our previous findings should apply for each one of the polarizations independently. Currently, the secondary modes are partially mitigated by tilting of both rectangular conductors at an angle $\theta_{boom} = 1°$. This allows for the boom to radiate part of the leaked power in a non-resonant manner, as it does not act as a perfect transmission line. A 3D view of the antenna has been presented in Figure 2a.

4.1. Individual Dipole Simulations

We first examine individual dipoles of the SKALA4.1 antenna, which present a secondary mode due to their triangular shape. The 5 longest triangular dipoles (15–19) are examined separately, as their secondary modes fall within the operational range of SKA-Low. For each of these dipoles, we choose our RLC parallel load values according to 3 design criteria:

1. The second order resonant frequencies, given by Equation 3 for each dipole and listed in Table 1.
2. The RLC resonant circuit Q-factor. It can be shown from circuit theory that Equation 4 reduces to $Q_{RLC,n} = R_n\sqrt{C_n/L_n}$, for the RLC load attached to the nth dipole. We would like to choose our bandwidth arbitrarily small, but this choice has practical issues since the tolerance of lumped elements cannot be zero. Thus, a value of $Q_{RLC,n} = 10$ was chosen as a compromise.
3. The value R_n is chosen, according to Equation 5, which accounts for the desired level of ohmic losses at the resonance frequency. Simulations were needed to test various R_n values and assess their effect, because there is no simple closed-form of Equation 5 for triangular dipoles.

In all the following simulations, FEKO commercial software is used, which implements the Method of Moments (https://altairhyperworks.com/feko/). To find suitable R_n values, the dipoles were modeled isolated and placed

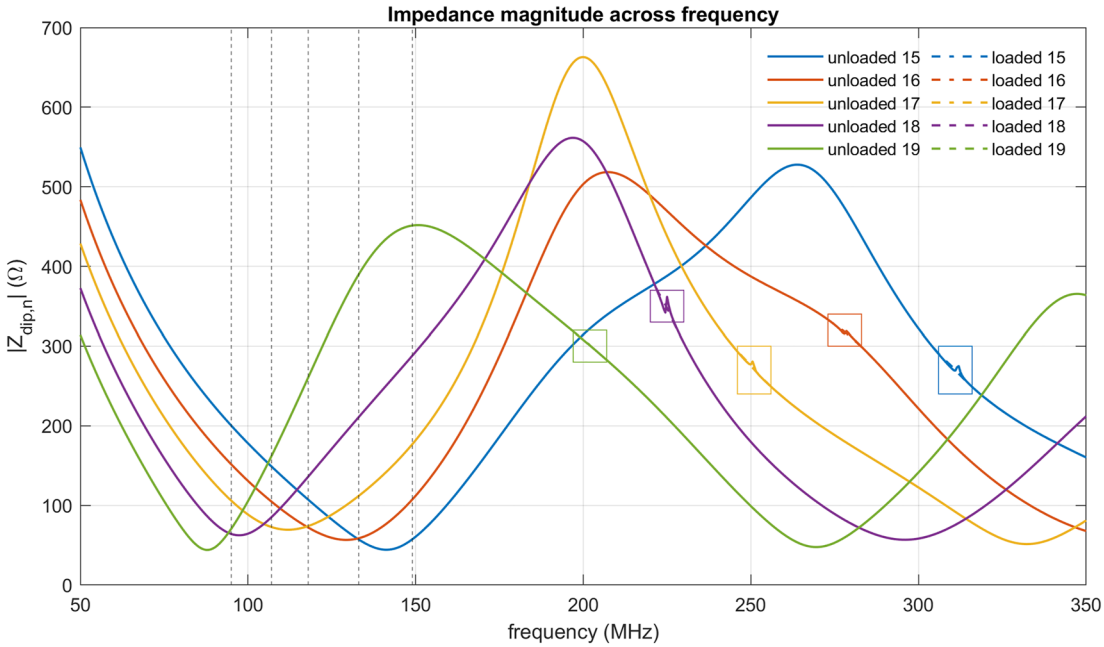

Figure 3. Simulated dipole impedance magnitude for unloaded and RLC loaded dipoles with an $R_n = 10\ \Omega$ in the operating frequency range of SKALA4.1. 10 curves are plotted, almost identical per 2, while the vertical lines indicate the $f_{n,1}$ of Table 1.

over a PEC, while excited at a wire port of characteristic impedance $Z_0 = 50\ \Omega$ connecting the triangular monopoles in their middle, with a fixed voltage set to $V_s = 1$ V. The two other ports seen with a red/blue polarity at the tip of the triangles are the loading positions. As an example, dipole 18 is depicted in Figure 2b, with its primary and secondary resonant currents are also plotted, while the x-axis values have been averaged for the corresponding mesh elements of the two triangle sides. We note the non-zero current on the two edges for the secondary resonance, as explained in Section 2. After assessing the impedance and current response, we have chosen a value of R_n such that the secondary mode no longer creates an impedance glitch, confirming that also for the gain pattern. The resistor value that seems to first show insignificant impedance and gain anomaly for all dipoles is $R_n = 10\ \Omega$.

We note that we did not further optimize the Q_n, R_n values (which are indicative more of the order of magnitude needed for the RLC circuits), since they were suitable for our simulations; higher Q's can also work but, as explained in Section 5, result in L values whose implemented components were not suitable for our prototypes. Higher R values might be needed for other antennas, but they would unavoidably induce more losses.

We first present the isolated dipole absolute impedance, to ascertain its behavior across the full frequency range when the load is added. Figure 3 contains a plot of all unloaded dipoles, and all loaded ones with an RLC of $R_n = 10\ \Omega$. The unloaded/loaded curves are indistinguishable per 2 for this scale of values, such that the load has a highly targeted effect; the glitches are highlighted in boxes. We have also confirmed the validity of the transmission line model for the impedance of short dipoles, since all of them have a strong reactive component and are close to the cotangent shape of Equation 1, up to frequency points close to the SKALA4.1 first resonances (vertical lines, see Table 1). The exact cut-off point of this model would have to result by a fit of the simulated data to the equation, which is out of our scope. It is also remarked that $|Z_{dip,n}|$ is influenced by the infinite PEC which is in some cases in the near field and thus interacting reactively.

In Figure 4 (top left), we present the calculated Q-factors for the unloaded dipoles, and the case of loaded ones with values $R_n = 10\ \Omega$. We use Equation 4 for all cases preceded by index n before $r = 2$, while also adding the loss resistance of Equation 5 for the loaded cases. All other subfigures zoom into the impedance glitch boxes of Figure 3 (color contours of Figure 3 correspond to box colors) to emphasize the desired mode suppresion. We can see from this plot that the calculated Q-factors drop below 5 with the addition of a load. Also note the apparent degeneracy of the calculated Q of dipole 19, which is low for all cases, along with the almost invisible glitch peak in the unloaded case. This could be a result of the closer near-field interaction of this dipole with the infinite ground plane.

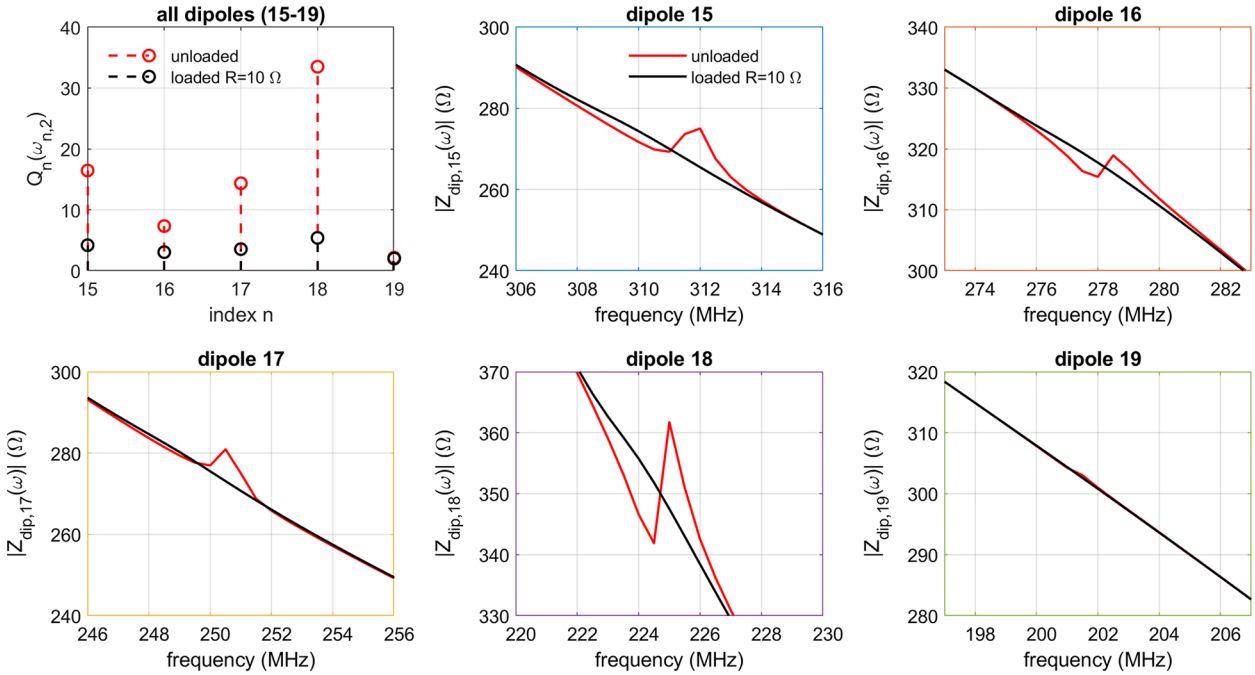

Figure 4. Calculated Q-factors of dipoles 15–19 (unloaded and loaded ones with an RLC of $R_n = 10\ \Omega$) of the SKALA4.1 antenna at frequencies $\omega_{n,2}$ (top left) and zoomed impedance glitches of (top right and the rest), whose color contour refers to the respective box of Figure 3.

The Q-factor calculation and impedance simulation serve mostly as an evaluation of the technique; the RLC circuit response as a filter is a typical bandpass curve, so relevant simulations are omitted (such a simulation curve can be found in Figure 7b of Section 4 for verification purposes during our laboratory experiments). Specific antenna designs could require the choice of arbitrary resistors and Q-factors for each dipole of the antenna; for SKALA4.1, these constant values perform quite well without the need for further optimization. It is evident from the analysis of this section that the secondary mode glitch is inherent to the dipoles.

4.2. SKALA4.1 Simulations

In previous simulations of SKALA4.1 (Bolli, Mezzadrelli, et al., 2020), dipoles 15 through 19 tested in the Section 4.1 were observed, first by means of their anomalous gain response, to be resonating with secondary modes at the frequencies listed in Table 1 (with a maximum amplitude of around 0.2 dB, as seen in Figure 5, "original SKALA4.1" curve). Also included in this table are the electric lengths of the dipoles at these frequencies, which are close to λ, and the respective amounts for the primary resonances. These are defined as local extrema of $\Re\{Z\}$ that satisfy $\Im\{Z'\} > 0$, as in Yaghjian and Best (2005), and have been extracted from simulated data of the antenna. We note the high accuracy of the theoretical approximations for both kinds of modes, with minor deviations for the primary modes as we anticipate in Section 3.2, due to dipole thickness and mutual coupling.

Further verification was made by examining the excited currents of the involved dipoles, as in Figure 2a for 229 MHz, where the full SKALA4.1 is displayed with a first active region which includes dipoles 10–12, while dipole 18 forms the second active region and is resonating with a secondary mode, which has a maximum current at the farthest points from the boom. The dynamic range has been chosen according to the maximum/minimum values, while the linear currents are shown in dBA to better emphasize their difference (which is around 30 dB).

We next incorporate the RLC circuits into the full SKALA4.1 antenna, and a simulation is run with FEKO in the full operating frequency range. Figure 5 shows our results in terms of antenna gain at zenith. The "original" label refers to the gain achieved with the unloaded antenna, while "RLC solution" label refers to our current loaded dipole solution. All dipoles 15–19 have been loaded in their respective edge (as in the ports of Figure 2b). As can be seen, due to the adjusted 1-dB dynamic range, we have managed to eradicate the anomalous feature.

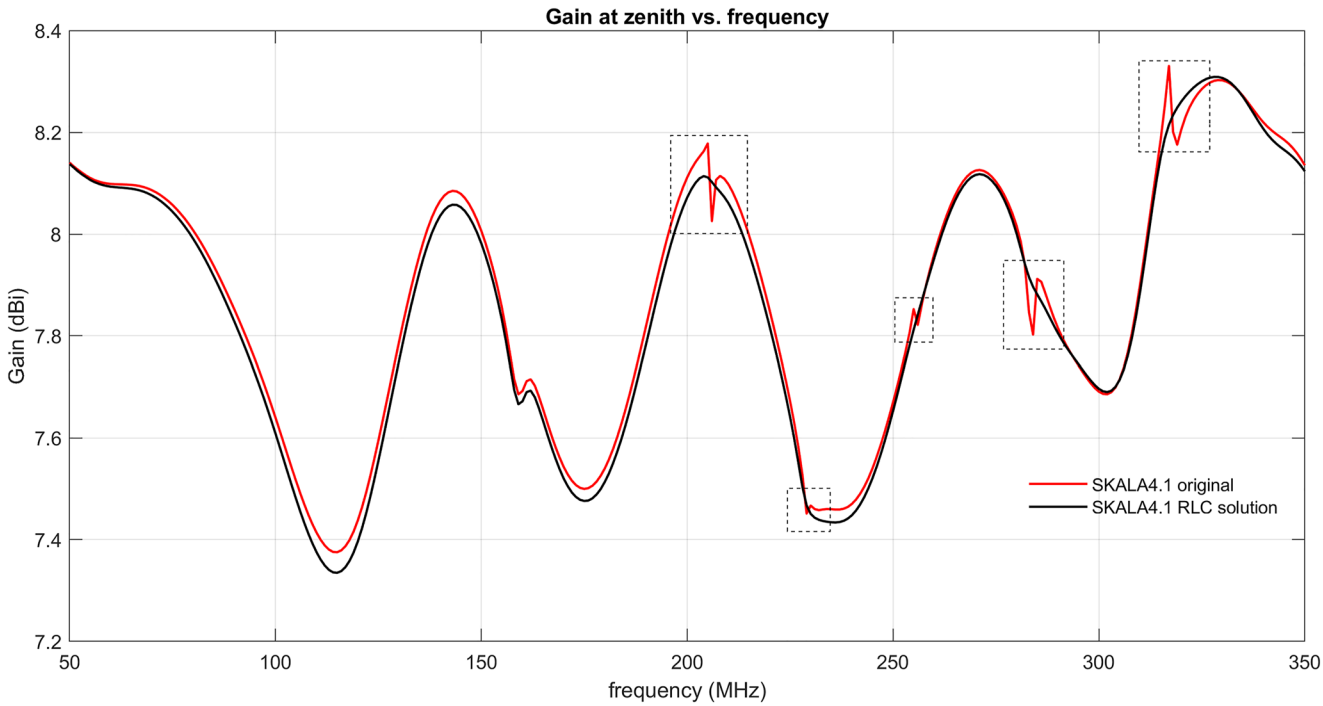

Figure 5. Gain in dBi at zenith for the SKALA4.1 X-polarized antenna for 2 different cases: unloaded (original SKALA4.1), RLC circuit loaded dipoles ($R_n = 10\ \Omega$). Dashed boxes are used to highlight the narrow-band glitches.

The cost on radiation efficiency is insignificant as well, and has been confirmed to be almost identical with the original antenna, which is less than 1% except for a drop in the lower frequencies due to aluminum losses (Bolli, Labate, et al., 2020). This is in any case visible in the slightly lower values for the RLC solution throughout the full frequency band. For completeness, another feature visible at 161 MHz is due to mutual coupling between the longest two dipoles (among which the bow-tie) (Wu et al., 2016); despite our attempts it has not been made possible to remedy this feature with the proposed RLC loading technique without worsening the antenna gain.

Finally, we also present some results in other spherical directions for the gain pattern. Figure 6 shows the gain response in the band 200–350 MHz for the same, "original" (left plot) and "RLC" loaded (right plot) antenna cases, at $\theta = 15°$ for the E- and H-plane ($\phi = 0°$ and $\phi = 90°$), as well as at $\theta = 30°$ for the H-plane. These directions were chosen such that all the gain values are comparable to each other and the glitches visible. It is concluded that, apart from a barely visible feature at $\theta = 30°$, $\phi = 90°$ and at 206 MHz, all other glitches are eradicated and the response appears smooth.

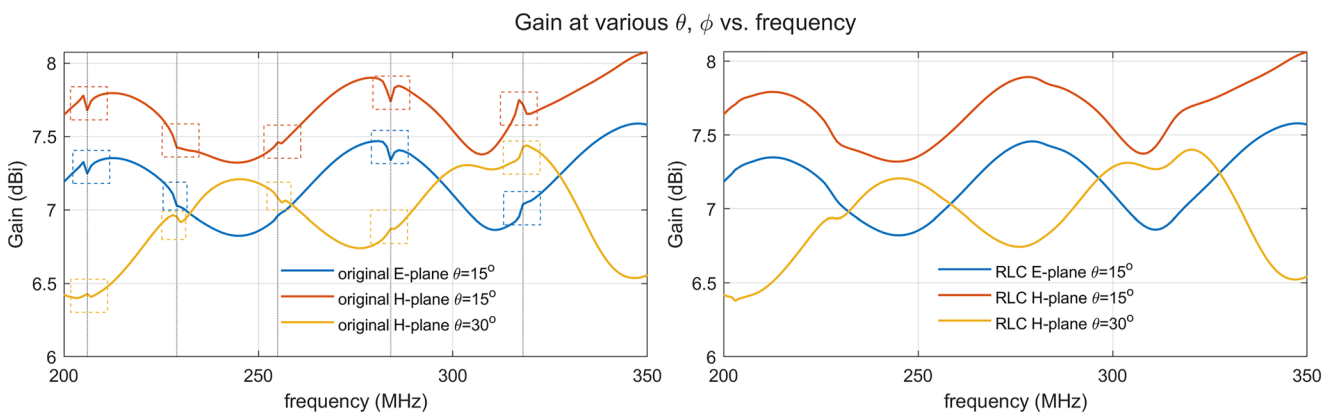

Figure 6. Gain in dBi at various θ, ϕ for the SKALA4.1 X-polarized antenna for 2 different cases: unloaded, original SKALA4.1 (left) and RLC circuit loaded dipoles (right). Dashed boxes are used to highlight the narrow-band glitches.

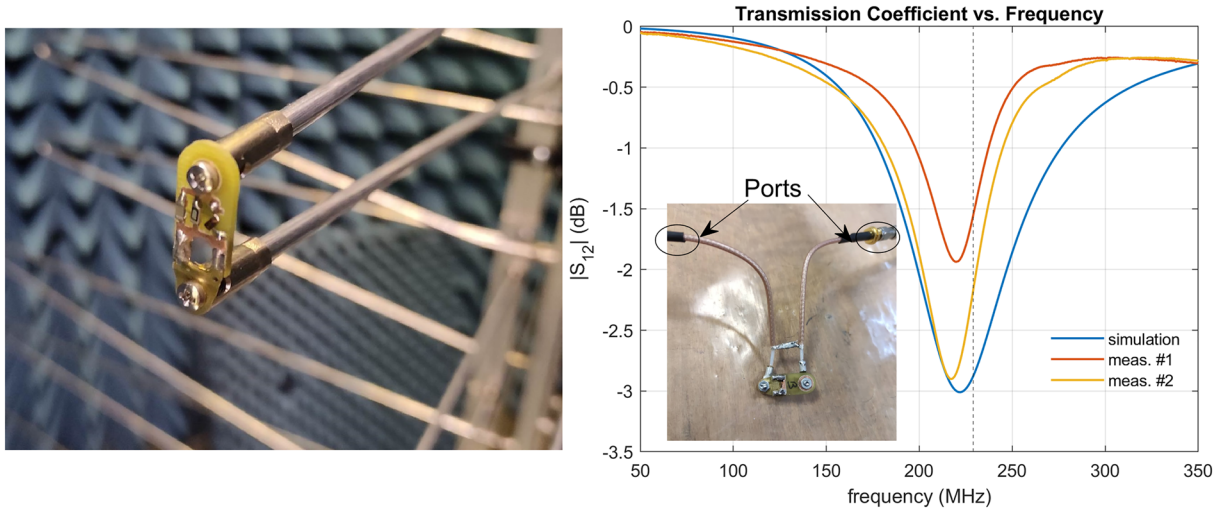

Figure 7. (a) Redesigned triangular dipole by Sirio Antenne, adding a screwable PCB on which RLC components are soldered, (b): RLC parallel circuit $|S_{21}|$ in dB, for a simulated circuit using $R = 100\ \Omega$, $L'_{18} = 15.59$ nH, $C'_{18} = 33$ pF and 2 measured prototypes (one of them shown as constructed in the image at the center-left) using the same values, which are observed to resonate at 217.5 MHz. A parasitic inductance $L_{18,p} = 8.44$ nH can account for an initially measured shift (not shown) from the designed resonance frequency, while the amplitude is variable among our 2 prototypes.

5. Experimental Verification

For the proposed RLC parallel circuit loading solution, we have attempted an experimental verification using a SKALA4.1 and replacing the dipoles responsible for the glitch phenomenon with new ones, designed in a custom way such that we could attach this type of load. Sirio Antenne (https://www.sirioantenne.it/it/), the contractor of antenna production for SKA-Low, has redesigned and manufactured these new dipoles. The practical solution for soldering the RLC circuit is a PCB element also designed by Sirio Antenne, a ≈ 2 cm long FR4 piece with conductive paths shown in Figure 7b, and also screwed on one of the dipoles in Figure 7a with its RLC components soldered.

5.1. RLC Circuit Measurement

To first measure and ascertain the performance of the RLC circuit as a 2-port device, we used an interface such as that shown at the center left of Figure 7b. Coaxial cable segments, the inner conductors of which were extended via circular rings on their free end (the other end containing their SMA), were used for compatibility with the VNA interface. These rings were screwed on the PCB, while a short-circuit connection of the outer conductors creates a virtual ground. We have also introduced a modification of the values of the loading circuit in order for a feasible prototype to be constructed. If one uses a resistor of $R_n = 10\ \Omega$ that was found in the previous section to be ideal, then the inductance values turn out to be very low (in the order of 100's of pH). This kind of component can only be implemented as a surface mount, which is hard to integrate in a parallel circuit manually, as we planned to do. We thus scaled the L_n values by one order of magnitude, which according to Equations 3 and 4 also means that C_n must be scaled down and R_n up by the same factor. That still allows for practical RC values, while a $R_n = 100\ \Omega$ resistor would induce some minor losses in the range 140–200 MHz.

To add to that complexity, it was further realised that parasitic components were inevitable in our manual RLC component integration on the PCB, which account for a shift in resonance frequency. For example, with an initial market inductance of $L_{18} = 7.15$ nH and a market capacitance of $C_{18} = 47$ pF used for constructing an initial circuit for the 18-th dipole, a parasitic $L_{18,p} = 8.44$ nH was calculated for a shift from the designed (229 MHz) to the initially measured (338 MHz) resonance, such that the actual inductance is $L'_{18} = L_{18} + L_{18,p} = 15.59$ nH. We should emphasize here that this PCB component was not optimized in its electric properties, and the soldering/screwing interfaces were expected to induce parasitics. Using a new value of $C'_{18} = 33$ pF, the new measured resonance, at 217.5 MHz, was the closest approach we could obtain to target the design frequency of 229 MHz. The constraint is set by C'_{18} as the closest standard market capacitance to the one obtained from Equation 3 by using L'_{18}, keeping the resonance fixed at the design frequency. Table 2 collects the $L_n^{(sim)}$, $C_n^{(sim)}$

Table 2
Simulation and Prototype Construction L, C Values

Dipole n	15	16	17	18	19
$L_n^{(sim)}$ (nH)	0.5	0.56	0.624	0.695	0.772
$C_n^{(sim)}$ (pF)	500.5	560.4	624.1	695	772.6
L_n (nH)	2.55	–	7.15	7.15	7.15
C'_n (pF)	20	–	24	33	44

Note. L_n and C'_n are market values. L_{16} and C'_{16} are omitted since an experimental verification was not possible for this dipole.

values that have been ideally used for each dipole in simulations in Section 4, the market inductances L_n used throughout, and the corrected market capacitances C'_n. These are the final values we used to construct the prototypes; the values C_n, L'_n are instead omitted since they are auxiliary for the correction procedure described above. It is reminded that, $R_n = 10\ \Omega$ and $R'_n = 100\ \Omega$ respectively, for all dipoles.

The example effective circuit (considering the R'_{18}, L'_{18}, C'_{18} values) was also simulated. Viewing it as a 2-port network with the coaxial cables corresponding to its ports, and a reference impedance of $Z_0 = 50\ \Omega$, a simple Z-to-S transformation results in $S_{21} = (2Z_0)/(Z_{RLC,18} + 2Z_0)$, using Equation 2 for $Z_{RLC,18}$. The $|S_{21}|$ of the simulated and measured RLC parallel load of 2 separate prototypes are presented for two constructed prototypes (meas. #1, meas. #2) in Figure 7b (design frequency at the vertical line). The shape of the resonance features of the two curves is in good agreement, while the amplitude varies at a level of ≈1 dB among the constructed prototypes; despite that, these circuits turned out to be useful in the antenna measurements.

5.2. SKALA4.1 Coupling Measurement

The experimental test that we have conducted is essentially similar to that of Kyriakou et al. (2021), a measurement of the coupling between a SKALA4.1 antenna and a transmitting VHF antenna, in terms of the scattering parameters of the system. The VHF antenna is a Yagi-Uda composed of 7 dipoles for receiving TV signals in the range of 180–260 MHz, so we have focused our measurement on the 3 first glitches as previously described, while the highest frequency one was also observed. A number of anechoic chamber experimental campaigns took place at the Arcetri Astrophysical Observatory in Florence, as can be seen in the photo of Figure 8a. Due to the limited dimensions of the anechoic chamber, the measurement is a near-field (reactive) one, with a horizontal pointing of the VHF antenna. The chamber was filled with extra absorbing panels on its floor, except for a cross-like area 1.6 m × 1.6 m that was occupied by a 5 cm-spaced rectangular grid acting as a ground plane. SKALA4.1 was excited along its Y-polarized dipoles, parallel to the dipoles of the VHF antenna, while its orthogonal polarization was terminated with a 50 Ω load, and an Agilent VNA was used to perform the measurement and save the data. Importantly, despite these differences from the simulations (non zenith pointing, non far-field regime), the glitch phenomenon clearly appears in our data.

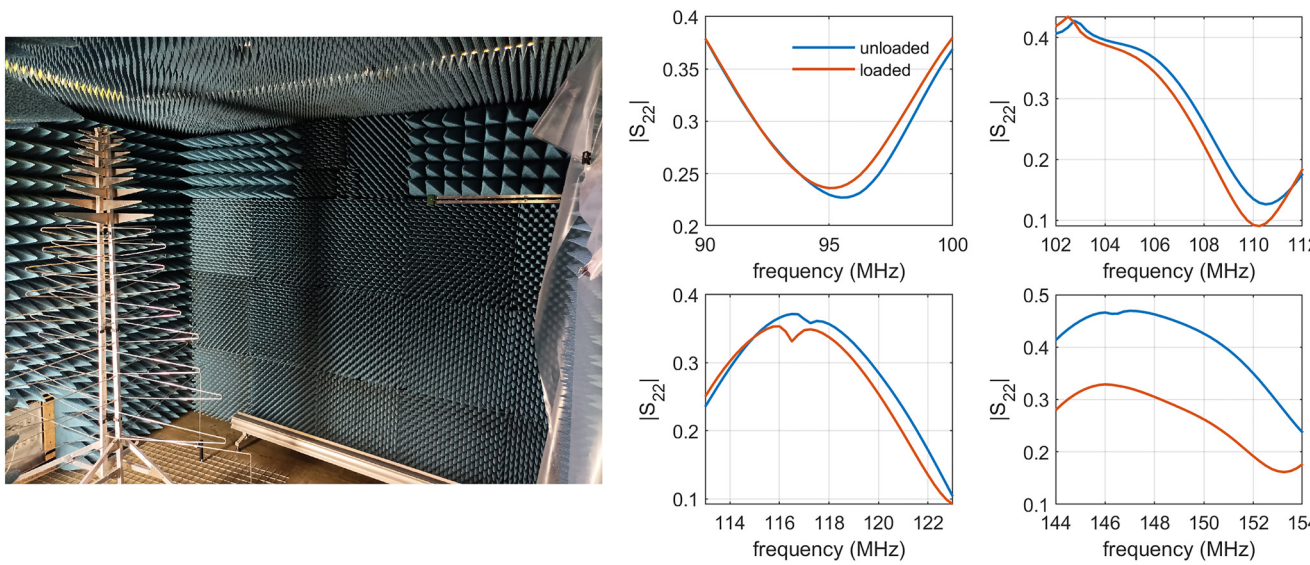

Figure 8. (a) Measurement configuration of a SKALA4.1 antenna and a VHF Yagi-Uda antenna at the Arcetri Astrophysical Observatory anechoic chamber, (b): $|S_{22}|$ VNA measurement, where port 1 is connected to a VHF antenna and port 2 is connected to a SKALA4.1 under two conditions: original, unloaded dipoles 19, 18, 17, and 15 (left to right and top to bottom), and the corresponding redesigned, loaded ones. The 4 frequency windows chosen correspond to a 10 MHz range around the primary resonance frequency of each dipole, listed in Table 1.

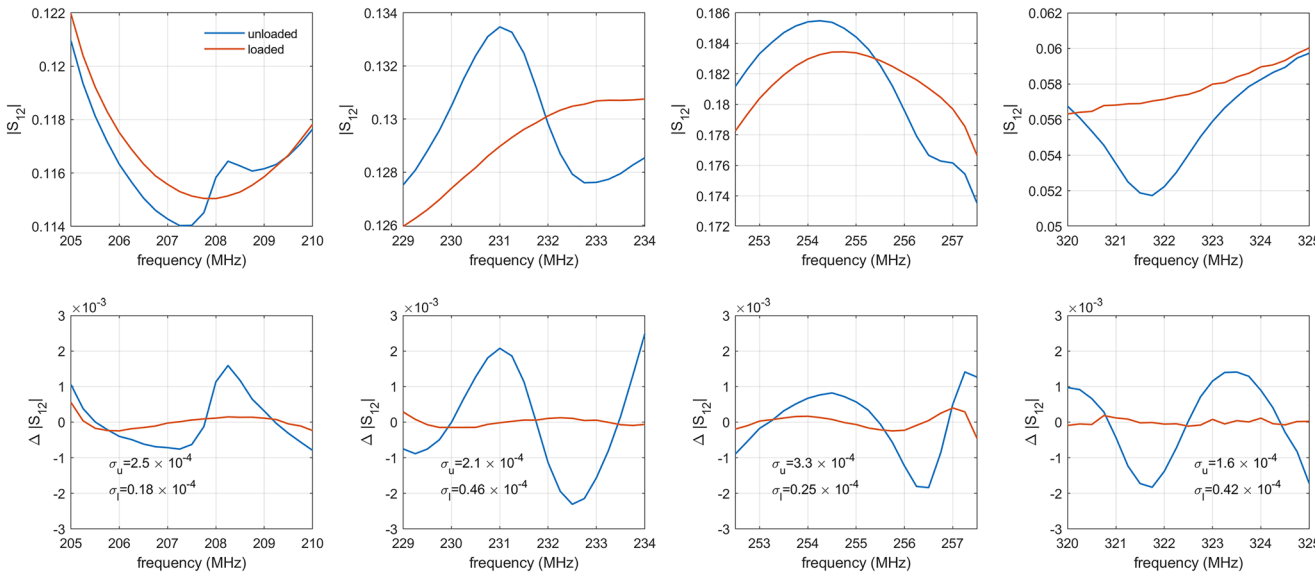

Figure 9. Top panels: $|S_{21}|$ measurement data, bandlimited to selected windows around each glitch of dipoles 19, 18, 17, 15 (left to right), Bottom panels: Residuals of the curves of the left panels after subtracting a polynomial fit of second degree to isolate the glitch from the smooth variation. Standard deviations are given on the lower left.

During the anechoic chamber measurements, we obtained two sets of results, each of them an ensemble average of 10 frequency sweeps without changing any measurement condition to reduce the random noise, since the horizon pointing provides a low level of coupling more susceptible to it. A fine resolution of 0.25 MHz was used. First, a set of measurements with the original dipoles of SKALA4.1 was made, while the next one was made after screwing the new, RLC-circuit loaded dipoles numbered 15, 17, 18, and 19. Intermediate measurements were also made after each dipole substitution to check the consistency of the results.

We first show in Figure 8b the measured $|S_{22}|$, in the four frequency windows around the primary resonances of the dipoles (as listed in Table 1), so as to test the immunity of the response out of the frequency bands where the glitches occur. It has to be emphasized that due to the anechoic chamber environment having a close proximity to the antenna, imperferct absorption and scattering from the VHF antenna, the measured reflection and log-periodic resonant frequencies do not closely follow that of (Bolli, Mezzadrelli, et al., 2020), which was a more precise measurement. However, it is evident that in the first 3 cases the shape is almost identical. The last panel is in the range of frequencies where the RLC load of dipole 19 should already attenuate and phase shift at an adequate level as to account for the apparent differences between the 2 curves.

For the second resonances, we will demonstrate the narrow-band $|S_{21}|$ measurement data in two ways: first, we show a zoom into a 5-MHz bandwidth to visually confirm their amplitude mitigation, as in the top panels of Figure 9. The features are small in amplitude (as Figure 4 has already suggested), but discernible from the otherwise smooth trend (only the last panels are more noisy, due to the lower level of coupling). As we have shown in previous results of this method of assessing the glitches in S_{21} measurements (Kyriakou et al., 2021), there are many differences between the anechoic chamber environment and a free-space simulation that is the most obvious way of a first approximation. We do not compare with simulation results here since it would be extremely challenging to introduce in the simulator the real operative conditions and reflection properties of the chamber walls. Therefore, the effectiveness of the proposed technique is here demonstrated by 2-step comparative measurements conducted on the antenna with and without the RLC load on the dipoles. A "differential" such analysis ensures that the reduction of the glitch could not have been produced by the anechoic panel or by the VHF antenna whose contributions are identical in the two consecutive measurements.

Second, for each of the two curves of Figure 9, we fit a second degree polynomial and examine the residuals shown in the bottom panels of Figure 9. This is a common method used in the de-embedding of instrumental effects on real radioastronomical data which, although different in our case (artificial source, coupling measurement and not far-field gain), can offer an insight on the smoothness of the curves (Raghunathan et al., 2021). On

the lower left corner of these panels we report the standard deviation over the bandwidth for both the unloaded/loaded curves (σ_{ull}). For this statistic measure to be comparable among the cases, the window has been selected such that the dynamic range of values does not change appreciably (≈0.01 for all cases), and the number of frequency points is also the same. It is verified that in all cases the loaded dipoles curve achieves a smoother trend with respect to the features resembling the glitches present in the unloaded dipoles curve. The residuals are always lower, as well as their standard deviation, a result which points to a smoother SKALA4.1 response under RLC dipole loading.

6. Conclusion

In this paper, we have presented a new way of tackling the problem of spurious radiation by a log-periodic dipole antenna owing to secondary modes of the constituent dipoles. The addition of a properly placed RLC parallel load at the maximum current position of these modes, has led to the dissipation of their energy on the resistor R, with a subsequent reduction of the total Q-factor at the resonant frequencies. For a full log-periodic antenna, the cost on radiation efficiency is negligible, since their modal amplitude is already quite low. Application is found on a SKALA4.1 antenna purposed as the array element of SKA-Low, where the low-frequency dipole glitches are eradicated in the sense of achieving gain smoothness. The last section presents the experimental verification of the method by means of anechoic chamber measurements of the S-parameters of a two-antenna system with a VHF antenna and a SKALA4.1 as its 2 ports.

Data Availability Statement

The `.dat`, `.mat` data and `.m` script (MATLAB) used for post-processing and visualisation in the study are available at Owncloud (institutional repository of INAF) via owncloud.ia2.inaf.it/index.php/s/3GsreZjnLyCS-jHs/download (https://doi.org/10.20371/INAF/DS/2023_00002). The electromagnetic model and mesh in `.cfx`, `.cfm` formats (operable in FEKO) are also included.

Acknowledgments
We would like to acknowledge the useful help of Giuseppe Virone in theoretically addressing the problem, the practical contribution of Renzo Nesti, Luca Cresci and Dario Panella in the antenna measurement campaigns, as well as that of Aldo Sonnini, Tommaso Lapucci and Giovanni Comoretto in the RLC prototype manufacturing and testing. Georgios Kyriakou would like to dedicate this paper in the memory of Sofia Alexouda, his fellow researcher and friend.

References

Balmain, K., & Nkeng, J. (1976). Asymmetry phenomenon of log-periodic dipole antennas. *IEEE Transactions on Antennas and Propagation*, *24*(4), 402–410. https://doi.org/10.1109/TAP.1976.1141380

Bantin, C., & Balmain, K. (1970). Study of compressed log-periodic dipole antennas. *IEEE Transactions on Antennas and Propagation*, *18*(2), 195–203. https://doi.org/10.1109/TAP.1970.1139650

Bolli, P., Labate, M. G., van Es, A., & Stringhetti, L. (2020). *Antenna & station performance update for SKALA4.1-al (Tech. Rep. No. SKA-TEL-SKO-0001099)*. Jodrell Bank Observatory: SKAO.

Bolli, P., Mezzadrelli, L., Monari, J., Perini, F., Tibaldi, A., Virone, G., et al. (2020). Test-driven design of an active dual-polarized log-periodic antenna for the square kilometre array. *IEEE Open Journal of Antennas and Propagation*, *1*, 253–263. https://doi.org/10.1109/OJAP.2020.2999109

Capek, M., Hazdra, P., & Eichler, J. (2012). A method for the evaluation of radiation q based on modal approach. *IEEE Transactions on Antennas and Propagation*, *60*(10), 4556–4567. https://doi.org/10.1109/TAP.2012.2207329

Carrel, R. (1961). The design of log-periodic dipole antennas. In *1958 IRE international convention record* (Vol. 9, pp. 61–75). https://doi.org/10.1109/IRECON.1961.1151016

Cheong, W.-M., & King, R. W. P. (1967). Log-periodic dipole antenna. *Radio Science*, *2*(11), 1315–1325. https://doi.org/10.1002/rds19672111315

de Lera Acedo, E., Razavi-Ghods, N., Troop, N., Drought, N., & Faulkner, A. J. (2015). SKALA, a log-periodic array antenna for the SKA-low instrument: Design, simulations, tests and system considerations. *Experimental Astronomy*, *39*(3), 567–594. https://doi.org/10.1007/s10686-015-9439-0

de Lera Acedo, E., & Wackley, B. (2017). SKALA3: An optimized antenna and LNA design for enhanced SKA1-LOW passband calibratability. Retrieved from ursi.org/proceedings/procGA17/papers/Paper_J5P-15(2055).pdf

De Vito, G., & Stracca, G. (1973). Comments on the design of log-periodic dipole antennas. *IEEE Transactions on Antennas and Propagation*, *21*(3), 303–308. https://doi.org/10.1109/TAP.1973.1140476

DuHamel, R., & Armstrong, M. (1966). Log-periodic transmission line circuits—Part I: One-Port circuits. *IEEE Transactions on Microwave Theory and Techniques*, *14*(6), 264–274. https://doi.org/10.1109/TMTT.1966.1126249

Gong, Z.-L., & Balmain, K. (1986). Reduction of the anomalous resonances of symmetric log-periodic dipole antennas. *IEEE Transactions on Antennas and Propagation*, *34*(12), 1404–1410. https://doi.org/10.1109/TAP.1986.1143776

Hassan, M. A., Al Jabri, A., & Al-Hakbani, K. (1991). Point-matching method for reduction of anomalous radiation of log-periodic dipole array. *Electronics Letters*, *27*(2), 1315–1317. https://doi.org/10.1049/el_19910827

He, H., Chen, Y., & Yang, S. (2019). Novel low profile ultra-wideband capacitance loaded log-periodic monopole array with reduced transverse dimension. *IET Microwaves, Antennas & Propagation*, *13*(9), 1443–1449. https://doi.org/10.1049/iet-map.2018.6012

Hilbert, M., Tilston, M., & Balmain, K. (1989). Resonance phenomena of log-periodic antennas: Characteristic-mode analysis. *IEEE Transactions on Antennas and Propagation*, *37*(10), 1224–1234. https://doi.org/10.1109/8.43530

Isbell, D. (1960). Log periodic dipole arrays. *IRE Transactions on Antennas and Propagation*, *8*(3), 260–267. https://doi.org/10.1109/TAP.1960.1144848

Jones, K., & Mayes, P. (1969). Continuously scaled transmission lines with applications to log-periodic antennas. *IEEE Transactions on Antennas and Propagation*, *17*(1), 2–9. https://doi.org/10.1109/TAP.1969.1139355

Kyriakou, G., Bolli, P., Subrahmanyan, R., & Davidson, D. B. (2021). Experimental verification of anomalous spectral features of SKALA4.1 antenna. In *2021 IEEE international symposium on antennas and propagation and usnc-ursi radio science meeting (APS/URSI)* (pp. 47–48). https://doi.org/10.1109/APS/URSI47566.2021.9704375

Labate, M. G., Braun, R., Dewdney, P., Waterson, M., & Wagg, J. (2017). SKA1-low: Design and scientific objectives. In *2017 XXXIInd general assembly and scientific symposium of the international union of radio science (URSI GASS)* (pp. 1–4). https://doi.org/10.23919/URSIGASS.2017.8105424

Labate, M. G., Dewdney, P., Braun, R., Waterson, M., & Wagg, J. (2017). The SKA low-frequency telescope: Performance parameters and constraints on the array configuration. In *2017 11th European conference on antennas and propagation (EUCAP)* (pp. 2259–2263). https://doi.org/10.23919/EuCAP.2017.7928622

Liang, P., & Wu, Q. (2018). Characteristic mode analysis of antenna mutual coupling in the near field. *IEEE Transactions on Antennas and Propagation*, *66*(7), 3757–3762. https://doi.org/10.1109/TAP.2018.2823867

McLean, J., Sutton, R., & Foltz, H. (2014). Investigation of the stop region of a compressed log-periodic dipole antenna. In *2014 IEEE antennas and propagation society international symposium (APSURSI)* (pp. 1314–1315). https://doi.org/10.1109/APS.2014.6904983

Mistry, K. K., Lazaridis, P. I., Zaharis, Z. D., & Loh, T. H. (2021). Design and optimization of compact printed log-periodic dipole array antennas with extended low-frequency response. *Electronics*, *10*(17), 2044. https://doi.org/10.3390/electronics10172044

Nyquist, D., & Chen, K. (1966). Traveling wave antenna with non-dissipative loading. In *1958 IRE international convention record* (Vol. 14, pp. 200–211). https://doi.org/10.1109/IRECON.1966.1147708

Raghunathan, A., Subrahmanyan, R., Shankar, N. U., Singh, S., Nambissan, J., Kavitha, K., et al. (2021). A floating octave bandwidth cone-disk antenna for detection of cosmic dawn. *IEEE Transactions on Antennas and Propagation*, *69*(10), 6209–6217. https://doi.org/10.1109/TAP.2021.3069563

Sheng, H., & Chen, Z. N. (2019). Radiation pattern improvement of cross-band dipoles using inductive-loading mode-suppression method. *IEEE Transactions on Antennas and Propagation*, *67*(5), 3467–3471. https://doi.org/10.1109/TAP.2019.2902649

Steiner, R., Ung, D. C. X., Hubrechsen, A., Jones, R. D., Wayth, R. B., Bentum, M. J., & Smolders, A. B. (2020). Optimizing processing time of radio-astronomy antenna simulations using FEKO. *Applied Computational Electromagnetics Society Journal*, *35*(10), 1153–1160. https://doi.org/10.47037/2020.aces.j.351007

Wu, Q., Su, W., Li, Z., & Su, D. (2016). Reduction in out-of-band antenna coupling using characteristic mode analysis. *IEEE Transactions on Antennas and Propagation*, *64*(7), 2732–2742. https://doi.org/10.1109/TAP.2016.2522459

Yaghjian, A., & Best, S. (2005). Impedance, bandwidth, and q of antennas. *IEEE Transactions on Antennas and Propagation*, *53*(4), 1298–1324. https://doi.org/10.1109/TAP.2005.844443

Zhao, J., Chen, Y., & Yang, S. (2018). In-band radar cross-section reduction of slot antenna using characteristic modes. *IEEE Antennas and Wireless Propagation Letters*, *17*(7), 1166–1170. https://doi.org/10.1109/LAWP.2018.2836926